ACS APPLIED MATERIALS & INTERFACES

Research Article

www.acsami.org

$Sr_{1.7}Zn_{0.3}CeO_4$: Eu^{3+} Novel Red-Emitting Phosphors: Synthesis and Photoluminescence Properties

Haifeng Li,[†,‡] Ran Zhao,[†,‡] Yonglei Jia,[†,‡] Wenzhi Sun,[†,‡] Jipeng Fu,[†,‡] Lihong Jiang,[†] Su Zhang,[†] Ran Pang,*[,†] and Chengyu Li*[,†]

[†]State key Laboratory of Rare Earth Resource Utilization, Changchun Institute of Applied Chemistry, Chinese Academy of Sciences, Changchun 130022, P. R. China.

[‡]University of Chinese Academy of Sciences, Beijing 100049, P. R. China.

ABSTRACT: A series of novel red-emitting $Sr_{1.7}Zn_{0.3}CeO_4$:Eu^{3+} phosphors were synthesized through conventional solid-state reactions. The powder X-ray diffraction patterns and Rietveld refinement verified the similar phase of $Sr_{1.7}Zn_{0.3}CeO_4$:Eu^{3+} to that of Sr_2CeO_4. The photoluminescence spectrum exhibits that peak located at 614 nm ($^5D_0$–$^7F_2$) dominates the emission of $Sr_{1.7}Zn_{0.3}CeO_4$:Eu^{3+} phosphors. Because there are two regions in the excitation spectrum originating from the overlap of the Ce^{4+}–O^{2-} and Eu^{3+}–O^{2-} charge-transfer state band from 200 to 440 nm, and from the intra-4f transitions at 395 and 467 nm, the $Sr_{1.7}Zn_{0.3}CeO_4$:Eu^{3+} phosphors can be well excited by the near-UV light. The investigation of the concentration quenching behavior, luminescence decay curves, and lifetime implies that the dominant mechanism type leading to concentration quenching is the energy transfer among the nearest neighbor or next nearest neighbor activators. The discussion about the dependence of photoluminescence spectra on temperature shows the better thermal quenching properties of $Sr_{1.7}Zn_{0.3}CeO_4$:0.3Eu^{3+} than that of Sr_2CeO_4:Eu^{3+}. The experimental data indicates that $Sr_{1.7}Zn_{0.3}CeO_4$:Eu^{3+} phosphors have the potential as red phosphors for white light-emitting diodes.

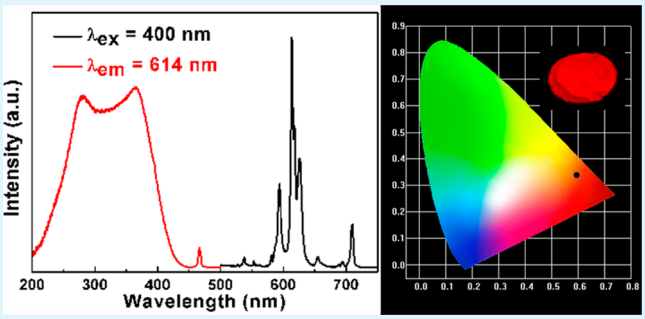

KEYWORDS: *red-emitting phosphors, photoluminescence, concentration quenching, thermal quenching*

1. INTRODUCTION

Currently, white light-emitting diodes (WLEDs) have drawn worldwide attention because of the compactness, high efficiency, good stability in physical and chemical properties, long operational lifetime, as well as energy saving and environmental protection.[1,2] WLEDs are widely used in the field of lighting and backlit lamps.[3,4] Moreover, the enormous progress made in the commercial LED chips with the near-UV light ranging from 350 to 420 nm has greatly boosted the research interest in phosphors excited efficiently within this range. Nowadays, the most prevalent way of fabricating WLEDs is to combine yellow-emission $Y_3Al_5O_{12}$:Ce^{3+} phosphors with commercial blue LED chips.[5] The characters of the simple combination have been shown by Jang et al.[6] Obviously, there exists a notable deficiency based on the tricolor theory. The drawback in red spectral region restricts the range of their application in several significant practical fields, especially as alternatives for the fields with lower color temperatures that dominate the lighting markets. In order to match well with the color requirements of lighting fields, novel red-emitting phosphors have been synthesized to improve the properties of the color temperatures and color rendering index (CRI). These near-UV light excited red-emitting phosphors are synthesized on the basis of Eu^{3+}-activated host, such as $CaYAl_3O_7$:Eu^{3+}[7] and La_2O_2S:Eu^{3+}.[8] Whereas some defects for them exist. For example, sulfide-based phosphors are chemically instable and moisture-sensitive. Hence, it is imperative to develop novel red-emitting phosphors excited effectively by near-UV light for lighting applications.

Sr_2CeO_4 reported by Danielson et al.[9] has an orthorhombic unit cell with Pbam as the space group.[10] The distinguishing feature of blue-white emission for the promising Sr_2CeO_4 phosphor is because of Ce^{4+}–O^{2-} charge-transfer state (CTS) band. There, however, exists a drawback for Sr_2CeO_4: the poor thermal stability.[11] The PL intensity declines greatly as the temperature ascends to 300 K. Meanwhile, Eu^{3+} ions show the corresponding emission owing to inner f–f transitions.[7,8] The Eu^{3+}-activated Sr_2CeO_4 phosphors exhibit characteristic emission of Eu^{3+} ions, which is influenced by the energy transfer between Ce^{4+}–O^{2-} CTS and Eu^{3+} ions. At the appropriate concentration of Eu^{3+} ions, the energy of Ce^{4+}–O^{2-} CTS can completely transfer to Eu^{3+} ions, resulting in the intense red emission. However, the limitation to Sr_2CeO_4:Eu^{3+} phosphors is the relevant narrow excitation band and poor thermal stability, which restrains their application range. It is, however, somewhat possible to get over the deficiency via the

Received: September 28, 2013
Accepted: February 18, 2014
Published: February 18, 2014

   dx.doi.org/10.1021/am4041493 | ACS Appl. Mater. Interfaces 2014, 6, 3163–3169

chemical substitution into the $(A)_2CeO_4$ orthorhombic structure, where the (A) cations are six-coordinated in octahedron.

Zn^{2+} ions are widely employed in the modification of the phosphors. There are many examples in the literatures, such as, the green-emission systems, $Li_2ZnGe_3O_8$:Mn,[12] LiZn-(PO_4):Mn,[13] and the orange-red-emission compounds, Ba_2ZnS_3,[14] and $CaZnGe_2O_6$:Mn.[15] In addition, Zn^{2+} ions can be doped into the luminescent materials serving as sensitizers or defect centers to enhance optical properties.[16,17] Consequently, a possible solution to boost the property of Sr_2CeO_4 is to substitute Zn^{2+} ions for part of Sr^{2+} ions on the condition that the Sr_2CeO_4 orthorhombic structure does not alter.

To our knowledge, insofar as the related research about the cerium−strontium−zinc oxide system is rarely reported. Therefore, in this work, we described a series of novel red-emitting $Sr_{1.7}Zn_{0.3}CeO_4$:Eu^{3+} phosphors which can meet the requirements of near-UV light induced red phosphors. The powder X-ray diffraction patterns and Rietveld refinement were employed to confirm the crystal and phase homogeneity of $Sr_{1.7}Zn_{0.3}CeO_4$:Eu^{3+}. The photoluminescence behaviors of the samples were discussed and then the photoluminescence intensity was compared with that of the commercial $Sr_2Si_5N_8$:Eu^{2+} phosphor. The mechanism type for the concentration quenching behavior and luminescence decay was studied systematically. Meanwhile, the thermal quenching properties were also discussed.

2. EXPERIMENTAL SECTION

2.1. Materials and Synthesis. A variety of red-emitting phosphors $Sr_{1.7-x}Zn_{0.3}CeO_4$:xEu^{3+} (SZC:xEu^{3+}, x = 0−0.5) were synthesized with the traditional high-temperature solid-state reactions. The starting materials $SrCO_3$ (A.R., 99.9%), CeO_2 (A.R., 99.9%), Eu_2O_3 (A.R., 99.99%), and ZnO (A.R., 99.9%) were weighted under the stoichiometric ratio. The raw materials were mixed and ground in an agate mortar thoroughly, and the homogenous mixtures were transferred to an alumina crucible and sintered at 1000 °C for 10 h in the air. Then, the pre-samples were re-ground and calcined at 1000 °C for 10 h again. After cooling to room temperature (RT) naturally, the as-obtained phosphors were ground into powder for the measurements.

2.2. Characterizations. The powder X-ray diffraction (XRD) profiles for phase identification were collected by using a D8 Focus diffractometer operating at 40 kV and 40 mA with graphite-monochromated Cu Kα radiation (λ = 0.15405 nm). In the process, the scanning rate is 10° min^{-1} with a 2θ ranging from 10 to 65°. A UV-3600 UV−vis−NIR spectrophotometer (Shimadzu, Japan) with the white powder $BaSO_4$ as a calibrated reference was used to perform the diffuse reflectance spectra. The photoluminescence excitation (PLE) and photoluminescence (PL) spectra of the phosphors were measured by a Hitachi F-7000 spectrophotometer with the excitation source of a 150W xenon lamp. The luminescence decay curves were obtained from a Lecroy Wave Runner 6100 Digital Oscilloscope (1 GHz) and a tunable laser (pulse width = 4 ns; gate = 50 ns) was utilized as the excitation source. The temperature dependence PL properties of the phosphors were recorded by an FLS-920-Combined Fluorescence Lifetime and Steady State Spectrometer (Edinburgh Instruments) with a 450 W xenon lamp as the excitation source. The quantum efficiency (QE) of the synthesized samples was measured by Photonic Multi-channel Analyzer C10027 (Hamamatsu, Japan). All the measurements were performed at RT unless otherwise mentioned.

3. RESULTS AND DISCUSSION

3.1. Phase Composition. The standard data of the single-phased crystal structure for Sr_2CeO_4 in the Joint Committee on Powder Diffraction Standards (JCPDS) card No. 50-0115 was used as the initial reference to explore the actual structure of the samples. The synthesized phosphors were analyzed via XRD to verify the phase composition of SZC:xEu^{3+}, as portrayed in Figure 1a associated with the standard data. It is

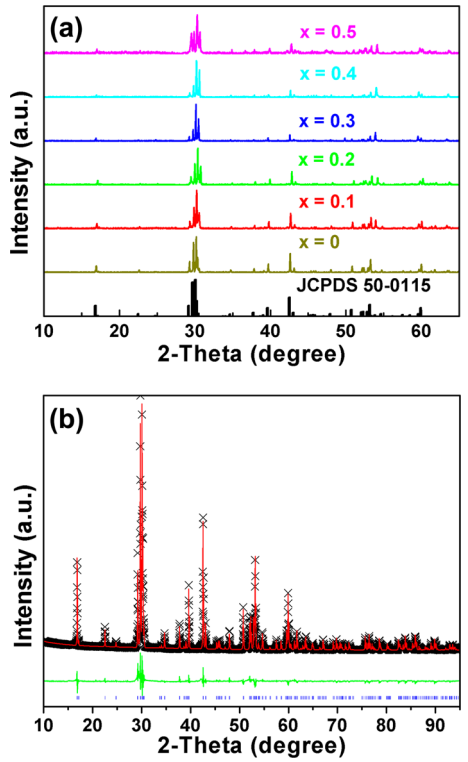

Figure 1. (a) XRD patterns of SZC:xEu^{3+} phosphors and the standard data for Sr_2CeO_4 (JCPDS No. 50-0115) as a reference. (b) Experimental (crosses) and calculated (red solid line) powder XRD patterns of $Sr_{1.7}Zn_{0.3}CeO_4$ matrix. The green solid lines represent the difference between experimental and calculated data and the blue sticks mark the Bragg reflections.

clear from Figure 1a that all XRD patterns agree well with the standard data of Sr_2CeO_4, which indicates that the phase formation of $Sr_{1.7}Zn_{0.3}CeO_4$ is the similar to that of Sr_2CeO_4 and the doped Eu^{3+} ions do not generate any notable impurities or lead to any obvious changes. However, the XRD peaks for SZC:xEu^{3+} phosphors shift to a larger 2θ angle compared with those of $Sr_{1.7}Zn_{0.3}CeO_4$ (SZC), which is ascribed to the cell shrink of the Sr_2CeO_4 (SCO) matrix by the substitution of Eu^{3+} (coordination number (CN) = 6, r = 1.206 Å) with an effective ionic radius that is smaller than that of Sr^{2+} (CN = 6, r = 1.32 Å).[18] As for SZC:xEu^{3+} phosphors, owing to the similar composition and crystal structure to SCO, the doped Eu^{3+} ions are also expected to preferably take the sites of Sr^{2+} ions and consequently caused the lattice shrink of the SZC matrix.

Figure 1b shows the experimental (black), calculated (red), and difference (green) XRD profiles for the Rietveld refinement of the $Sr_{1.7}Zn_{0.3}CeO_4$ matrix. The refinement finally converging to χ^2 = 9.71, R_{wp} = 7.61%, and R_p = 5.19% is shown in Table 1. $Sr_{1.7}Zn_{0.3}CeO_4$ has an orthorhombic unit cell with *Pbam* as the space group and cell parameters a = 6.109765 Å, b = 10.301090 Å, c = 3.577259 Å, and cell volume (V) = 225.143 $Å^3$. The lattice constants decrease with the introduction of Zn^{2+} ions when compared with the parameters of pure Sr_2CeO_4.[10]

3.2. Reflectance and Photoluminescence Properties of Eu^{3+}-Doped $Sr_{1.7}Zn_{0.3}CeO_4$. Figure 2a depicts the

Table 1. Rietveld Refinement and Crystal Data of $Sr_{1.7}Zn_{0.3}CeO_4$

formula	$Sr_{1.7}Zn_{0.3}CeO_4$
formula weight	745.342
space group	*Pbam* (No. 55)
a (Å)	6.109765
b (Å)	10.301090
c (Å)	3.577259
units, *Z*	2
V (Å^3)	225.143
crystal density (g cm^{-3})	5.499
χ^2	9.71
R_p (%)	5.19
R_{wp} (%)	7.61

reflectance spectra of SZC and SZC:Eu^{3+}. The SZC host shows an absorption band ranging from 200 to 380 nm with two peaks at approximate 261 and 323 nm that corresponds to the Ce^{4+}−O^{2-} CTS band due to the two distinct sites of O^{2-} ions for the octahedral CeO_6 in the SZC host and the reflectance spectral tail is at 380 nm. However, the reflectance spectrum of SZC:Eu^{3+} phosphors consists of two parts. One part is the remarkable broad absorption range from 200 to 440 nm with the peaks at around 261 and 350 nm, which may be assigned to the overlap of Ce^{4+}−O^{2-} and Eu^{3+}−O^{2-} CTS band. Meanwhile, the other is the characteristic absorption at 463 and 536 nm of Eu^{3+} ions owing to the intra-4f transitions. It is also observed from the reflectance spectrum of SZC:Eu^{3+} phosphors that the reflectance spectral margin at 440 nm moves to a lower location in comparison with that of SZC, which may be due to the Eu^{3+}−O^{2-} CTS band.

Figure 2b illustrates the absorption spectrum of $Sr_{1.7}Zn_{0.3}CeO_4$ calculated by using the Kubelka−Munk theoretic formula. The band gap of the $Sr_{1.7}Zn_{0.3}CeO_4$ host can be estimated according to the equation[19]

$$[F(R_\infty)h\nu]^n = C(h\nu - E_g) \quad (1)$$

where $h\nu$ represents the energy per photon, C is a proportional constant, E_g is the value of the band gap, n = 1/2 means a indirect allowed transition, 2 represents a direct allowed transition, 3/2 stands for a direct forbidden transition, or 3 indicates an indirect forbidden transion, $R_\infty = R_{sample}/R_{standard}$, and $F(R_\infty)$ is the Kubelka−Munk function, which is defined as[20]

$$F(R_\infty) = (1 - R)^2/2R = K/S \quad (2)$$

In the above equation, K, R, and S are the absorption, reflectance, and scattering parameter, respectively. From the extrapolation of the line for $[F(R_\infty)h\nu]^2 = 0$, the estimated value of E_g was about 3.37 eV.

Figure 3 shows the PLE spectra of SZC:Eu^{3+} and SZC monitored at 614 and 460 nm, respectively. The figure clearly

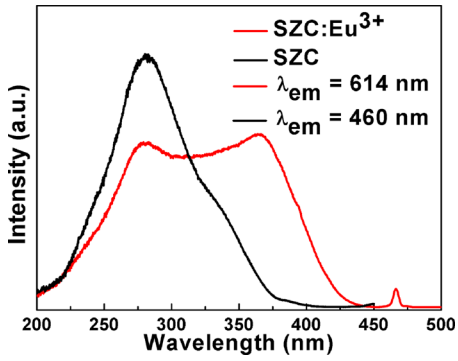

Figure 3. PLE spectra of SZC and SZC:Eu^{3+} phosphors.

presents the change of PLE spectra between SZC and SZC:Eu^{3+}. For SZC, the PLE spectrum consists of two excited states at 281 and 322 nm, which are attributed to the t_{1u}−f and t_{1g}−f CTS band, respectively. In terms of the reason for CTS band, Nag et al.[21] studied the nature of the luminescence for Sr_2CeO_4 and found that the empty electronic structure of 4f shell and the environment of Ce^{4+} ions make the Ce^{4+}−O^{2-} CTS band possible. However, the PLE spectrum of SZC:Eu^{3+} becomes wider and exhibits a broad absorption range from 200 to 440 nm with two peaks at around 280 nm and 363 nm, which may be assigned to the overlap of Eu^{3+}−O^{2-} CTS band and Ce^{4+}−O^{2-} CTS band. G. Blasse[22] studied the influence of the CTS band on the luminescence properties and found that the CTS band may be related to the distance between the ligand and the central ion. The longer the distance is, the more energy it needs to excite the CTS band. The results from the Rietveld refinement show the incorporation of Zn^{2+} into Sr_2CeO_4 leads to the decrease of the volume of the lattice, while it does not change the orthorhombic structure of Sr_2CeO_4. The lattice shrink may result in the decline of the average length of Sr^{2+}−O^{2-} by comparison with that for pure Sr_2CeO_4. Therefore, we propose the average length of Eu^{3+}−O^{2-} may

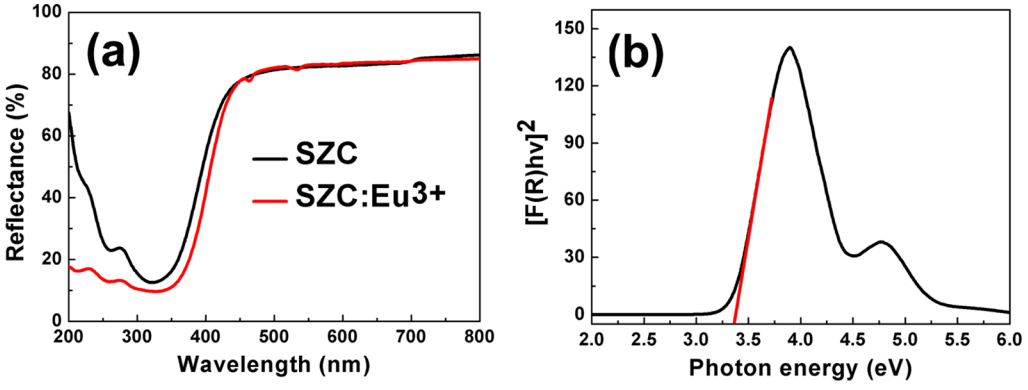

Figure 2. (a) UV−vis diffuse reflectance spectra of SZC and SZC:Eu^{3+} (b) absorption spectra of $Sr_{1.7}Zn_{0.3}CeO_4$ matrix calculated by the Kubelka−Munk equation.

dx.doi.org/10.1021/am4041493 | ACS Appl. Mater. Interfaces 2014, 6, 3163−3169

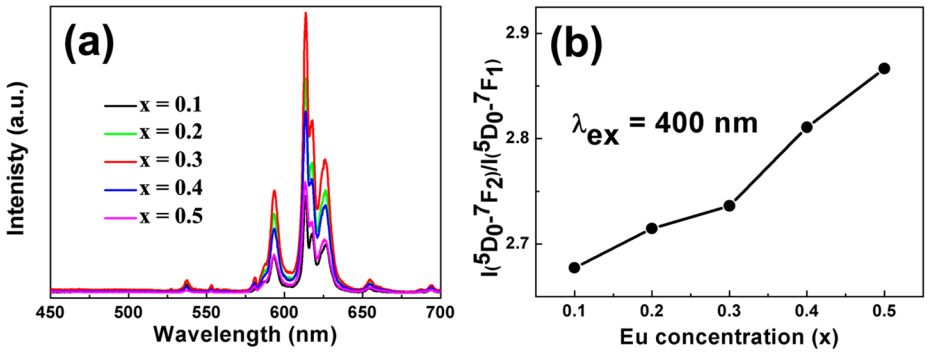

Figure 4. (a) Dependence of PL spectra of SZC:xEu^{3+} phosphors on Eu^{3+} ions concentrations x (λ_{ex} = 400 nm). (b) Relationship of PL intensity ratio $I(^5D_0 \rightarrow {}^7F_2)/I(^5D_0 \rightarrow {}^7F_1)$ with the doped Eu^{3+} ions concentrations x (λ_{ex} = 400 nm).

decrease when Eu^{3+} replaces Sr^{2+}, which makes the Eu^{3+}−O^{2-} CTS band possible. From Figure 3, one can also see that the excitation spectrum almost coincides with the reflectance one. The difference in shape between the excitation and reflectance spectra of Ce^{4+}−O^{2-} and Eu^{3+}−O^{2-} CTS band may be ascribed to that the CTS absorption only partly makes contribution to the $^5D_0 \rightarrow {}^7F_2$ emission. Meanwhile, there are a shoulder peak at 395 nm and a sharp line at 467 nm due to the intra-4f transitions for Eu^{3+} ions: $^7F_0$ to $^5L_6$, $^5D_2$, respectively. The PLE spectrum of SZC:Eu^{3+} phosphors indicates that the phosphors are perfectly consistent with the commercial near-UV LED chips. Consequently, $Sr_{1.7}Zn_{0.3}CeO_4$:Eu^{3+} phosphors have the potential to be employed as a near-UV light excited red-emission phosphors for WLEDs.

Figure 4a exhibits that the PL spectra of SZC:xEu^{3+} phosphors vary with the doped Eu^{3+} ions concentrations under 400 nm excitation. The phosphors show characteristic emission of Eu^{3+} ions with a strongest peak centered at 614 nm, which concurs with the $^5D_0$−$^7F_2$ electronic dipole transition of Eu^{3+} ions. There are also other peaks at 626, 618, 594, 581, 553, and 537 nm, which are attributed to $^5D_0$−$^7F_3$, $^5D_0$−$^7F_2$, $^5D_0$−$^7F_1$, $^5D_0$−$^7F_0$, $^5D_1$−$^7F_2$, and $^5D_1$−$^7F_1$ transitions of Eu^{3+} ions, respectively. Furthermore, little emission from Ce^{4+}−O^{2-} CTS band occurs, indicating a fully energy migration from Ce^{4+}−O^{2-} CTS band to Eu^{3+} emitting centers. Due to the reason that most of the trivalent lanthanides are shielded by outer electrons of 5s and 5p, the inner 4f transitions for them are weakly influenced by ligand environment of crystals.[23] Hence, it is also observed that the line shape of emission spectrum varies little with Eu^{3+} ions concentrations. Meanwhile, the Commission International de L'Eclairage (CIE) chromaticity coordinate (0.60, 0.34) for SZC:xEu^{3+} phosphors can be obtained from the emission spectra, which is almost consistent with the National Television System Committee (NTSC) primary rule for the red emission.

Transitions that are sensitive to the crystal environment are called hypersensitive ones. The $^5D_0 \rightarrow {}^7F_2$ transition is hypersensitive to the environment of the crystal field, while the $^5D_0 \rightarrow {}^7F_1$ transition is insensitive. Meanwhile, the magnetic dipole $^5D_0 \rightarrow {}^7F_1$ transition is predominant in a position with an inversion symmetry, while the $^5D_0 \rightarrow {}^7F_2$ electronic transition becomes the strongest one in a location without an inversion symmetry.[24−27] Thus, the PL intensity ratio between $^5D_0 \rightarrow {}^7F_2$ (614 nm) and $^5D_0 \rightarrow {}^7F_1$ (594 nm) transitions is a good way to probe the matrix structure. In general, the high ratio of $I(^5D_0 \rightarrow {}^7F_2)/I(^5D_0 \rightarrow {}^7F_1)$ provides the conclusion that the Eu^{3+} ions occupy positions with a low symmetry and no inversion center. Figure 4b shows the ratio dependence of $I(^5D_0 \rightarrow {}^7F_2)/I(^5D_0 \rightarrow {}^7F_1)$ on Eu^{3+} ions concentrations. One can clearly see that the rate of $I(^5D_0 \rightarrow {}^7F_2)/I(^5D_0 \rightarrow {}^7F_1)$ always goes up with the ascendment of the doped Eu^{3+} ions concentrations (x = 0.1−0.5) excited at 400 nm. The result indicates that the introduction of Eu^{3+} ions into $Sr_{1.7}Zn_{0.3}CeO_4$ would perturb the symmetry of the matrix structure. It is also clear that the $^5D_0 \rightarrow {}^7F_2$ transition dominates the PL spectra of SZC:xEu^{3+} (x = 0.1−0.5) phosphors under 400 nm excitation, which implies that Eu^{3+} ions would mainly occupy positions without an inversion symmetry.

Figure 5 exhibits the comparison between the PL spectra of SZC:0.3Eu^{3+} phosphor and the commercial red-emitting

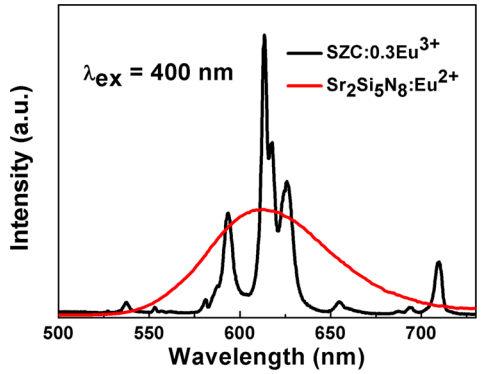

Figure 5. PL spectra of SZC:0.3Eu^{3+} phosphor (λ_{ex} = 400 nm) and that of the commercial red-emitting $Sr_2Si_5N_8$:Eu^{2+} phosphor (λ_{ex} = 400 nm).

$Sr_2Si_5N_8$:Eu^{2+} phosphor both under 400 nm excitation. Although the $Sr_2Si_5N_8$:Eu^{2+} phosphor exhibits about 85.1% wider area than the studied phosphor owing to the typical sharp emission of Eu^{3+} ions, the PL intensity for the $^5D_0 \rightarrow {}^7F_2$ transition for the SZC:0.3Eu^{3+} phosphor is 163.5% higher than that of $Sr_2Si_5N_8$:Eu^{2+} phosphor. In addition, the QE recorded under 366 nm excitation of SZC:0.3Eu^{3+} phosphor and $Sr_2Si_5N_8$:Eu^{2+} phosphor was 46.1% and 78.2%, respectively. However, the observed low QE of SZC:0.3Eu^{3+} phosphor may be further boosted by optimizing the synthesis process.

3.3. Concentration Quenching Properties of Eu^{3+}-Doped $Sr_{1.7}Zn_{0.3}CeO_4$. The dependence of PL spectra for SZC:xEu^{3+} phosphors on various Eu^{3+} ions concentrations excited at 400 nm is shown in Figure 4a. For SZC:xEu^{3+} phosphors, the PL intensity ascends with the rising of Eu^{3+} ions

concentrations up to x = 0.3 and declines beyond that concentrations, which is ascribed to the concentration quenching behavior. On the basis of the percolation energy transfer theory,[28−30] concentration quenching phenomenon mainly results from two mechanism types: (1) Interactions between Eu^{3+} ions, which leads to energy reabsorpted by the neighboring Eu^{3+} ions and (2) Energy migration from a percolation bunch of Eu^{3+} ions to quenching centers.

Therefore, the critical distance R_c between Eu^{3+} ions can be approximately calculated via the following equation obtained by Blasse:[31]

$$R_C \approx 2\left[\frac{3V}{4\pi X_C N}\right]^{1/3} \quad (3)$$

Where N represents the value of available sites that Eu^{3+} ions can occupy per unit cell, X_C is the critical concentration for Eu^{3+} ions, and V is the volume per unit cell. For SZC:$x$$Eu^{3+}$ phosphors, N = 3.4, V = 225.14 Å^3, and X_C = 0.3, then the proximate calculated value of R_c is 7.50 Å which is much larger than the critical distance of 3.60 Å between Eu^{3+} ions.

As the cross-relaxation process through the exchange interaction type usually comes into effect under a certain distance (the typical R_c is ∼4 Å) in a forbidden transition for Eu^{3+} ions, and the excitation and emission spectra do not overlap very well,[32] energy transfer among Eu^{3+} ions in SZC:$x$$Eu^{3+}$ phosphors is not triggered by the exchange interaction type, but through the non-radiative energy migration interaction mechanism. The non-radiative energy migration between Eu^{3+} ions usually occurs because of the electric multipolar−multipolar interaction which has an intimate relationship with the distance on the basis of Dexter's theory.[33] The change of the PL intensity can be usually used to account for the multipole−multipole interaction type if the energy migration process takes place between the identical sort of activators. The PL intensity (I) per activator follows the formula[34,35]

$$I/x = k[1 + \beta(x)^{\theta/3}]^{-1} \quad (4)$$

where x represents the activator concentration; θ = 3 indicates the energy migration among nearest neighbor or next nearest neighbor activators, while θ = 6, 8, and 10 corresponds to the dipole−dipole, dipole−quadrupole, or quadrupole−quadrupole interaction, respectively; k and β are constants per interaction for a given matrix excited under the same condition. By simplifying eq 4, we can obtain that the relationship of lg[I/x(Eu^{3+})] with lg[x(Eu^{3+})] is linear with a slope of θ/3. Furthermore, Figure 6 plots the relationship of lg[I/x(Eu^{3+})] with lg[x(Eu^{3+})] to understand the concentration quenching. According to Figure 6, the slope of the fitting line is −1.04. On the basis of the slope, the value of θ is calculated to be 3.13 roughly equal to 3. The result implies that the dominant mechanism type resulting in the concentration quenching behavior for Eu^{3+} ions in SZC:$x$$Eu^{3+}$ phosphors is the energy transfer among the nearest neighbor or next nearest neighbor activators.

3.4. Luminescence Lifetime Properties of Eu^{3+}-Doped $Sr_{1.7}Zn_{0.3}CeO_4$.

To further probe the energy migration process, the luminescence decay curves of Eu^{3+} ions were measured and then the luminescence lifetimes of the phosphors were studied. Figure 7 portrays the concentration dependence of decay curves for the $^5D_0 \rightarrow {}^7F_2$ transition on various Eu^{3+} ions in SZC:$x$$Eu^{3+}$ phosphors excited at 400 nm and monitored

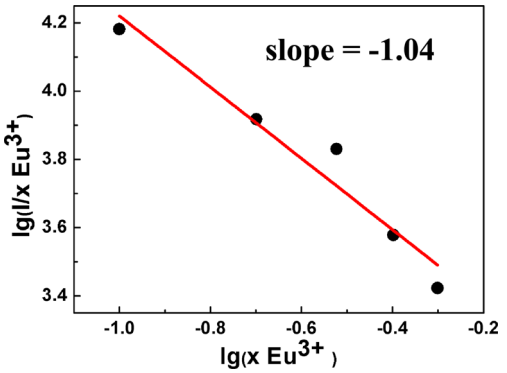

Figure 6. Relationship of lg(I/$x$$Eu^{3+}$) with lg($x$$Eu^{3+}$) in SZC:$x$$Eu^{3+}$ phosphors under 400 nm excitation.

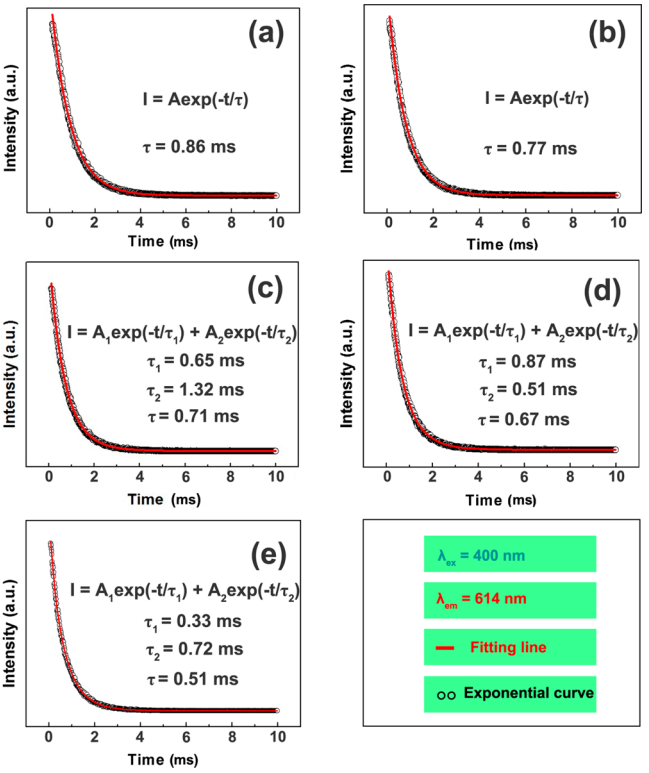

Figure 7. Luminescence decay curves of the $^5D_0 \rightarrow {}^7F_2$ transition and the fitting exponential lines for various Eu^{3+} ions concentrations of x = (a) 0.1, (b) 0.2, (c) 0.3, (d) 0.4, and (e) 0.5 in SZC:$x$$Eu^{3+}$ phosphors.

at 614 nm together with the corresponding fitting exponential lines. Usually, the distance between activators declines when their concentrations go up. Thus, the energy transfer process between activators comes into effect substantially, which acts as an extra luminescence decay approach. Consequently, the decay time could be affected by the energy migration process between activators in the host. Meanwhile, the relaxation rate of the extra energy-migration way may be different, which results in the decay curves exhibiting not a mono-exponential decay. If there is no interaction between Eu^{3+} ions, the decay curve is a mono-exponential function.[36−38] From Figure 7, When Eu^{3+} ions concentrations are below 0.3, the decay curves can be perfectly fitted by the single exponential decay equation

$$I = A\ \exp(-t/\tau) \quad (5)$$

dx.doi.org/10.1021/am4041493 | ACS Appl. Mater. Interfaces 2014, 6, 3163−3169

where I means the luminescence intensity, A represents the constant, and t and τ are the time and the decay constant of the exponential component, respectively. The single exponential decay curves imply little energy migration between Eu^{3+} ions.

However, when concentrations are up to 0.3, decay curves for Eu^{3+} ions deviate from the mono-exponential rule and can be best fitted using the double exponential formula

$$I = A_1 \exp(-t/\tau_1) + A_2 \exp(-t/\tau_2) \quad (6)$$

where A_1 and A_2 represent constants, I is the luminescence intensity, t is the time, and τ_1 and τ_2 are decay constants of exponential aspects. The double exponential decay curves indicate the possible interactions between Eu^{3+} ions.

Meanwhile, the decreasing lifetime presented in Figure 7a–e of the $^5D_0 \rightarrow {}^7F_2$ transition with the increasing Eu^{3+} ions concentrations further exhibits the trend of the energy transfer between Eu^{3+} ions.

3.5. Thermal Quenching Properties of Eu^{3+}-Doped $Sr_{1.7}Zn_{0.3}CeO_4$. The thermal stability of the phosphor plays a significant role in WLEDs applications. The dependence of PL spectra for SZC:0.3Eu^{3+} phosphor under 400 nm excitation on temperature is depicted in Figure 8a. The PL intensity of the phosphor declines with the increase of temperature ranging from 294 to 494 K, which indicates the temperature quenching behavior. The relative peak intensity of SZC:0.3Eu^{3+} phosphor declined by 84.3% of the initial intensity at 494 K. The activation energy (E_a) can be calculated through the relationship of the PL intensity with temperature by using the formula[39]

$$\ln\left(\frac{I_o}{I}\right) = \ln A - \frac{E_a}{k_B T} \quad (7)$$

where I and I_o represent the PL intensity of SZC:0.3Eu^{3+} phosphor at the experimental temperature and RT, respectively; A is constant and does not influence the calculation; and k_B is Boltzmann's constant (8.617×10^{-5} eV/K). From eq 7, we can obtain the relationship of $\ln(I_o/I)$ with $1/T$ is linear with the slope value of $-(E_a/k_B)$. Figure 8b shows the profile for the dependence of $\ln(I_o/I)$ on $1/T$. According to Figure 8b, the calculated value of E_a was 0.1788 eV which is bigger than that of Sr_2CeO_4:Eu^{3+} (E_a = 0.1355 eV). The inset in Figure 8a shows the relationship of the relative PL intensity of SZC:0.3Eu^{3+} and Sr_2CeO_4:Eu^{3+} with temperature. It is clearly that the thermal quenching of SZC:0.3Eu^{3+} is better than Sr_2CeO_4:Eu^{3+}. The result indicates that the SZC:0.3Eu^{3+} phosphor has the potential as a red phosphor for WLEDs applications.

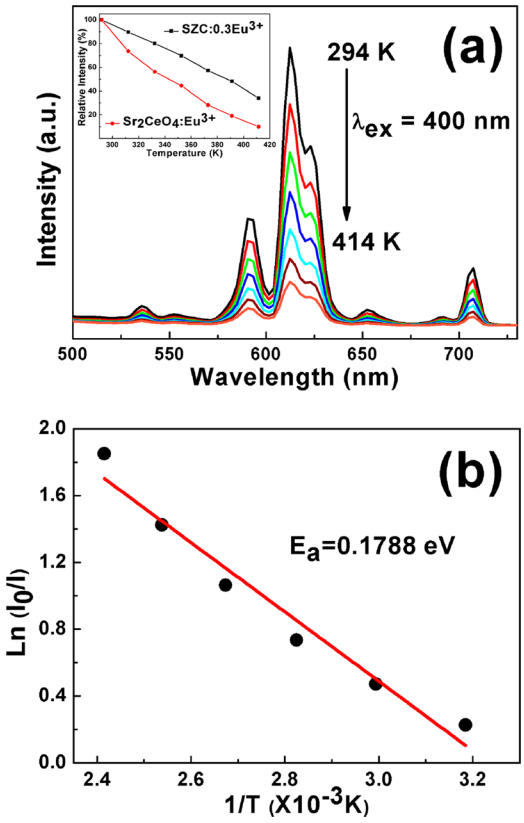

Figure 8. (a) Dependence of PL spectra for SZC:0.3Eu^{3+} phosphor with temperature (λ_{ex} = 400 nm). The inset in (a) shows the relative PL intensity of SZC:0.3Eu^{3+} and Sr_2CeO_4:Eu^{3+} phosphors as a function of temperature. (b) Profile on the dependence of $\ln(I_o/I)$ on $1/T$ for SZC:0.3Eu^{3+} phosphor.

4. CONCLUSION

A series of novel red-emitting Eu^{3+}-doped $Sr_{1.7}Zn_{0.3}CeO_4$ phosphors have been synthesized. The powder X-ray diffraction patterns and Rietveld refinement show that $Sr_{1.7}Zn_{0.3}CeO_4$ has an orthorhombic crystal structure with the space group *Pbam* and lattice constants a = 6.109765 Å, b = 10.301090 Å, c = 3.577259 Å, and V = 225.143 Å^3. The peak located at 614 nm ($^5D_0 - {}^7F_2$) predominates the PL spectrum of $Sr_{1.7}Zn_{0.3}CeO_4$:Eu^{3+} with CIE coordinate (0.60, 0.34) almost consistent with NTSC primary rule for the red emission. Because of the broad excitation band originating from the overlap of the $Ce^{4+}-O^{2-}$ and $Eu^{3+}-O^{2-}$ CTS band from 200 to 440 nm, and from the intra-4f transitions with a shoulder peak at 395 nm and a sharp line at 467 nm, the phosphor could be well excited by the near-UV light. On the basis of the investigation of PL properties for synthesized phosphors, the conclusion is made that the dominant mechanism type leading to the concentration quenching of Eu^{3+} is the energy transfer among the nearest neighbor or next nearest neighbor activators. The study about the dependence of PL spectra on temperature indicates the better thermal quenching property of SZC:0.3Eu^{3+} than that of Sr_2CeO_4:Eu^{3+}. All of the experimental results indicate that Eu^{3+}-doped $Sr_{1.7}Zn_{0.3}CeO_4$ phosphors may be promising as red phosphors for WLEDs applications.

AUTHOR INFORMATION

Corresponding Authors

*E-mail: pangran@ciac.ac.cn.

*E-mail: cyli@ciac.ac.cn.

Notes

The authors declare no competing financial interest.

ACKNOWLEDGMENTS

The research was supported by the Fund for Creative Research Groups (Grant 21221061).

REFERENCES

(1) Kim, J. S.; Jeon, P. E.; Choi, J. C.; Park, H. L.; Mho, S. I.; Kim, G. C. *Appl. Phys. Lett.* **2004**, *84*, 2931.

(2) Im, W. B.; Kim, Y. I.; Fellows, N. N.; Masui, H.; Hirata, G. A.; Den, S. P.; Seshadri, B. R. *Appl. Phys. Lett.* **2008**, *93*, No. 091905.

(3) Uchida, Y.; Taguchi, T. *Opt. Eng.* **2005**, *44*, 124003.

(4) Bachmann, V.; Ronda, C.; Meijerink, A. *Chem. Mater.* **2009**, *21*, 2077.
(5) Sohn, K. S.; Park, D. H.; Cho, S. H.; Kwak, J. S.; Kim, J. S. *Chem. Mater.* **2006**, *18*, 1768.
(6) Jang, H. S.; Im, W. B.; Lee, D. C.; Jeon, D. Y.; Kim, S. S. *J. Lumin.* **2007**, *126*, 371.
(7) Park, S. H.; Lee, K. H.; Unithrattil, S.; Yoon, H. S.; Jang, H. G.; Im, W. B. *J. Phys. Chem. C* **2012**, *116*, 26850.
(8) Tian, Y.; Qi, X.; Wu, X.; Hua, R.; Chen, B. *J. Phys. Chem. C* **2009**, *113*, 10767.
(9) Danielson, E.; Devenney, M.; Giaquinta, D. M.; Golden, J. H.; Haushalter, R. C.; McFarland, E. W.; Poojary, D. M.; Reaves, C. M.; Weinberg, W. H.; Wu, X. D. *Science* **1998**, *279*, 837.
(10) Danielson, E.; Devenney, M.; Giaquinta, D. M.; Golden, J. H.; Haushalter, R. C.; McFarland, E. W.; Poojary, D. M.; Reaves, C. M.; Weinberg, W. H.; Wu, X. D. *J. Mol. Struct.* **1998**, *470*, 229.
(11) van Pieterson, L.; Soverna, S.; Meijerink, A. *J. Electrochem. Soc.* **2000**, *147*, 4688.
(12) Palumbo, D. T.; Brown, J. J. *J. Electrochem. Soc.* **1970**, *117*, 1184.
(13) Chan, T. S.; Liu, R. S.; Baginskiy, I. *Chem. Mater.* **2008**, *20*, 1215.
(14) Thiyagarajan, P.; Kottaisamy, M.; Ramachandra Rao, M. S. *J. Phys. D: Appl. Phys.* **2006**, *39*, 2701.
(15) Che, G.; Liu, C.; Li, X.; Xu, Z.; Liu, Y.; Wang, H. *J. Phys. Chem. Solids* **2008**, *69*, 2091.
(16) Chung, S. M.; Kang, S. Y.; Shin, J. H.; Cheong, W. S.; Hwang, C. S.; Cho, K. I.; Lee, S. J.; Kim, Y. J. *J. Cryst. Growth* **2011**, *326*, 94.
(17) Singh, V.; Rai, V. K.; Ledoux-Rak, I.; Badie, L.; Kwak, H. Y. *Appl. Phys. B* **2009**, *97*, 805.
(18) Meng, Q. L.; Lee, C. i; Ishihara, T.; Kaneko, H.; Tamaura, Y. *Int. J. Hydrogen Energy* **2011**, *36*, 13435.
(19) Jiang, Z.; Wang, Y.; Wang, L. *J. Electrochem. Soc.* **2010**, *157*, J155.
(20) Morales, A. E.; Mora, E. S.; Pal, U. *Rev. Mex. Fis.* **2007**, *53*, 18.
(21) Nag, A.; Kutty, T. R. N. *J. Mater. Chem.* **2003**, *13*, 370.
(22) Blasse, G. *Struct. Bonding (Berlin)* **1976**, *26*, 43.
(23) Shionoya, S.; Yen, W. M. *Phosphor Handbook*; CRC Press: Boca Raton, FL, 1999; pp 88 and 179.
(24) Banerjee, A. K.; Mukhopadhyay, A. K.; Mukherjee, R. K.; Chowdhury, M. *Chem. Phys. Lett.* **1979**, *67*, 418.
(25) Wang, J. W; Chang, Y. M; Chang, H. C; Lin, S. H; Huang, L. C. L; Kong, X. L; Kang, M. W. *Chem. Phys. Lett.* **2005**, *405*, 314.
(26) Jia, M.; Zhang, J.; Lu, S.; Sun, J.; Luo, Y.; Ren, X.; Song, H.; Wang, X. J. *Chem. Phys. Lett.* **2004**, *384*, 193.
(27) Wei, Z.; Sun, L.; Liao, C.; Yin, J.; Jiang, X.; Yan, C.; Lü, S. *J. Phys. Chem. B* **2002**, *106*, 10610.
(28) Huang, C. H.; Chen, T. M. *Inorg. Chem.* **2011**, *50*, 5725.
(29) Vyssotsy, V. A.; Gordon, S. B.; Frisch, H. L.; Hammersley, J. M. *Phys. Rev.* **1961**, *123*, 1566.
(30) Deng, D.; Yu, H.; Li, Y.; Hua, Y.; Jia, G. *J. Mater. Chem. C* **2013**, *1*, 3194.
(31) Blasse, G. *Philips Res. Rep.* **1969**, *24*, 131.
(32) Im, W. B.; Fellows, N. N.; DenBaars, S. P.; Seshadri, R.; Kim, Y. I. *Chem. Mater.* **2009**, *21*, 2957.
(33) Dexter, D. L.; Schulman, J. H. *J. Chem. Phys.* **1954**, *22*, 1063.
(34) Van Uiter, L. G. *J. Electrochem. Soc.* **1967**, *114*, 1048.
(35) Ozawa, L.; Jaffe, P. M. *J. Electrochem. Soc.* **1971**, *118*, 1678.
(36) Fang, Y. C.; Huang, X. R.; Juang, Y. D.; Chu, S. Y. *J. Am. Ceram. Soc.* **2011**, *95*, 1613.
(37) Sohn, K. S.; Choi, Y. Y.; Park, H. D. *J. Electrochem. Soc.* **2000**, *147*, 1988.
(38) Chien, C. H.; Kuo, T. W.; Chen, T. M. *Appl. Mater. Interface* **2010**, *2*, 1395.
(39) Fonger, W. H.; Struck, C. W. *J. Chem. Phys.* **1970**, *52*, 6364.